ACS APPLIED MATERIALS & INTERFACES

www.acsami.org Research Article

# Time-Resolved Mechanism of Positive Aging in InP Quantum-Dot Light-Emitting Diodes

Sung-Yoon Joe,[§] Beomhee Yoon,[§] Doyoon Shin, Wan Ki Bae, Sang-Shin Lee,* and Hyunho Lee*

Cite This: https://doi.org/10.1021/acsami.4c10646 Read Online

ACCESS | Metrics & More | Article Recommendations | Supporting Information

**ABSTRACT:** Positive aging has been reported to be effective for enhancing electroluminescence characteristics of quantum dot (QD) based optoelectrical devices. This study investigated the intricate mechanisms underlying the positive aging effect in quantum-dot light-emitting diodes (QLEDs) influenced by encapsulation with ultraviolet-curable resin. A 120-h analysis assessed the impact of the resin on the electron transport layer and emission layer, utilizing a strategically positioned perfluorinated ionomer (PFI) interlayer. The PFI layer effectively delayed the $Al_2O_3$ formation at the zinc magnesium oxide (ZMO)/Al interface and further reduced the interactions within the QD/ZMO interface, thereby curtailing exciton quenching at the interfaces. The time-sequential effect of positive aging demonstrated that resin encapsulation effectively passivates the ZMO surfaces after 12 h. The positive aging facilitated the reaction between aluminum and oxygen from ZMO, contributing to $Al_2O_3$ formation within 48 h of aging. Furthermore, positive aging passivated the defect states of the QD surface and the QD/ZMO interface, reducing exciton quenching at the QD or QD/ZMO interface. The enhanced electron injection and reduced exciton quenching resulted in aged InP QLEDs, exhibiting an external quantum efficiency of 12.04%. This is a significant increase from the 3.16% observed in the control device. Finally, a sequential mechanism of positive aging in InP QLEDs was devised, providing new insights into the time-related operation of aging agents. This study elucidates an advanced time-resolved mechanism of positive aging, thereby offering valuable insights into the intricate dynamics of excitons within the domain of QLED physics.

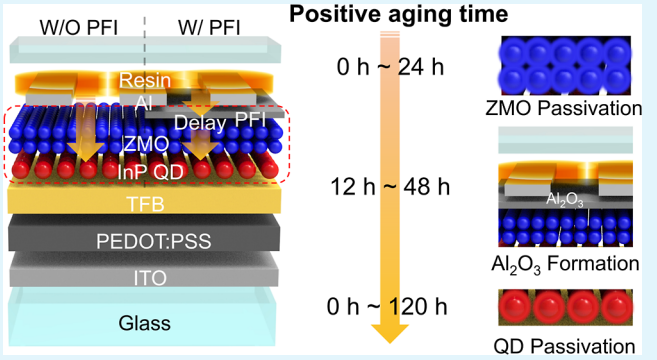


**KEYWORDS:** *InP, QLED, positive aging, UV-curable resin, encapsulation*



## INTRODUCTION

Quantum-dot (QD) light-emitting diodes (QLEDs) are promising candidates for next-generation display applications owing to their excellent optoelectronic properties, such as tunable emission colors by varying the QD size and composition, low driving voltage, high color purity, and low-cost solution fabrication.[1−10] The external quantum efficiencies (EQE) of blue, green, and red QLEDs were significantly improved from 0.01[11] to over 20%[12−14] (21.4, 27.6, and 23.1%, respectively), similar to those of conventional organic light-emitting diodes (OLEDs). Thus, QLEDs are considered potential successors in wide-color-gamut display applications.[15] A critical consideration for the high-performance QLEDs is effectively controlling the charge injection balance and exciton dynamics at the interface. A charge injection imbalance impairs the QLED performance, leading to issues such as Auger recombination and current leakage.[16−18]

QLEDs are encapsulated using an ultraviolet (UV)-curable resin glue to improve their device performance and stability.[19] Acid components in resin, which are considered to cause device degradation in OLEDs, positively affect the device and are referred to as positive aging in QLEDs.[20] A positive aging effect is defined as the enhancement of the electroluminescence (EL) performance of QLEDs encapsulated with a UV-curable resin over time. Acharya et al. demonstrated that this phenomenon of increasing QLED efficiency over time could be caused by the reduced defect density of ZnO by the reaction of the ZnO electron transport layer (ETL) with the encapsulation resin to form zinc carbonate.[20] Similarly, positive aging has been attributed to factors such as interfacial reactions between the Al cathode and ZnMgO nanoparticle (ZMO) ETL, leading to changes, such as aluminum oxide ($AlO_x$) formation and oxygen vacancy creation in ZMO.[9] The oxygen vacancies in ZMO can be passivated by acrylic acid from a UV-curable resin.[16,21] These interfacial reactions enhance electron

Received: June 27, 2024
Revised: August 15, 2024
Accepted: August 16, 2024

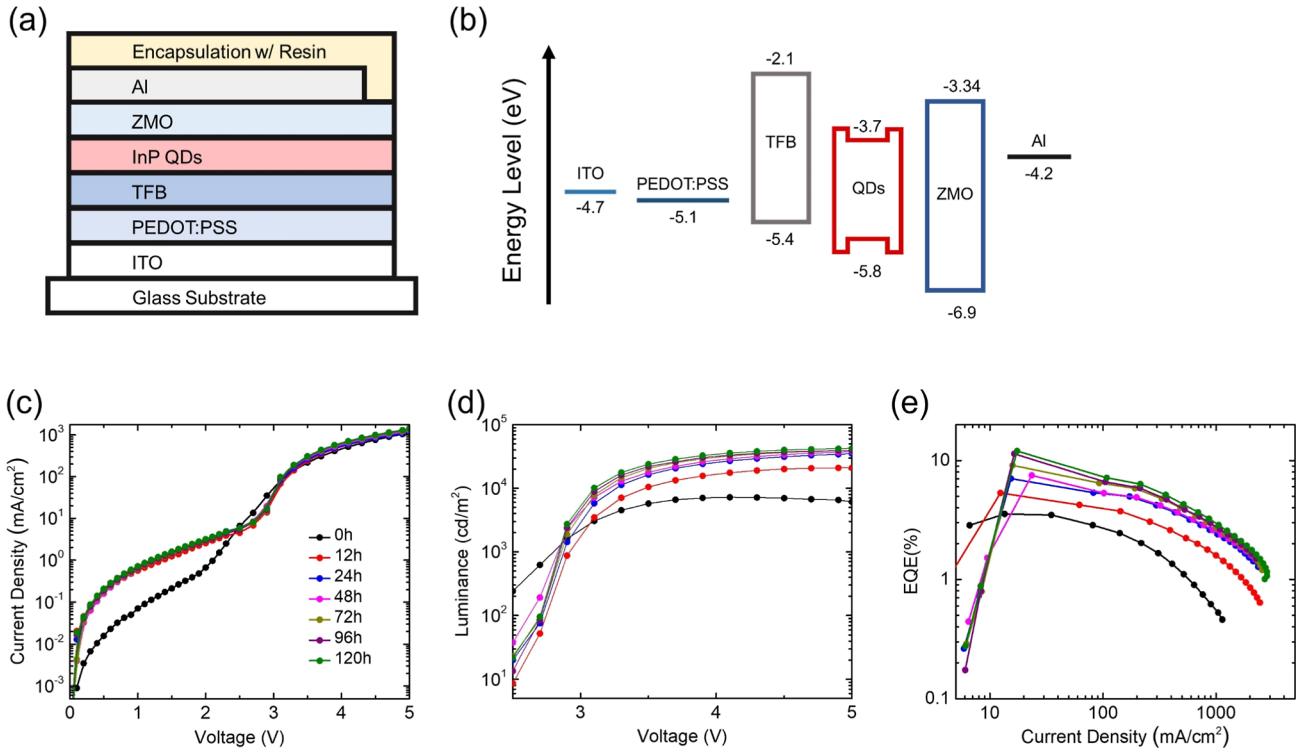


**Figure 1.** (a) Device structure, (b) energy band diagram, (c) $J-V$, (d) $L-V$, (e) EQE$-J$ results according to various positive aging time changes of QLEDs with resin induced encapsulation.

injection and suppress exciton quenching, increasing EQE.[9,22] Despite the extensive research and advancements in positive aging, a detailed understanding of the mechanisms of sequential resin infiltration through devices, particularly in terms of luminance and EQE, remains relatively unexplored. Accordingly, time-resolved investigation of the effect of positive agent (in the resin) infiltration through the device should be investigated.

This study investigated the positive aging mechanism based on the aging time of a QLED device by a UV-curable resin. A perfluorinated ionomer (PFI) insulating interlayer was strategically inserted at the desired interfaces in the device to intentionally delay the infiltration of the positive agents. The PFI delayed the positive reactions, thereby inhibiting exciton quenching on the spots. Consequently, the time sequence of positive agent infiltration was coupled with the variation of EL characteristics regarding aging time. Meanwhile, the general positive aging mechanism on the device constituent layers was further investigated. The ZMO surfaces were effectively passivated by positive aging, which diminished the exciton quenching from the QDs. Moreover, positive aging facilitated the reaction of Al with oxygen from ZMO, forming $Al_2O_3$, which effectively inhibited the electron leakage path. Furthermore, positive aging passivated the QD surface and QD/ZMO interface, enhancing radiative recombination within the QD core. Owing to the balanced charge injection and suppression of exciton quenching at the defect states, the positively aged InP QLEDs exhibited EQEs of 12.04%, significantly increasing from 3.16% for the control device. Finally, a sequential mechanism of positive aging in InP QLEDs was suggested, providing new insights into the time-related operation of aging agents.

## RESULTS AND DISCUSSION

Figure 1 shows the performance variations of the InP QLEDs throughout the aging process. The positive aging method is described in the Experimental section. The structure of the QLED depicted in Figure 1a comprises a multilayer stack arranged on a glass substrate comprising indium tin oxide (ITO), poly(3,4-ethylenedioxythiophene) polystyrenesulfonate (PEDOT:PSS), poly[(9,9-dioctylfluorenyl-2,7-diyl)-*co*-(4,4′-(*N*-(4-*sec*-butylphenyl)diphenylamine))] (TFB), InP QD, ZMO, and Al, subsequently capped with resin for encapsulation. The energy band diagram presented in Figure 1b elucidates the energy levels between each layer of the QLED, providing insights into the injection and transport mechanisms of charge carriers. Figure 1c illustrates the progressive increase in the current density and voltage ($J-V$) characteristics with aging time. The increase in current density over time indicates an alteration in the charge injection mechanism and transfer between the electrode and the conductive layer. The measured current density at 4 V increased from an initial value of 463 mA/cm$^2$ (at an aging time of 0 h) to 867 mA/cm$^2$ after 120 h. This was presumed to be due to the reduced resistance of the charge transport layer and nonradiative recombination caused by the traps within the QDs and QD interfaces. Figure 1d shows the changes in luminance and voltage ($L-V$) with aging time. The maximum luminance gradually increased from 7113 cd/m$^2$ (at an aging time of 0 h) to 35,830 cd/m$^2$ after 120 h, implying enhanced internal quantum efficiency due to the reduced exciton quenching effect by passivating ZMO and QD layers.[1,2,6] Figure 1e shows the progression of the device EQE and current density (EQE$-J$) with aging time. At the low voltage regime, the luminance and EQE can be measured higher in case of 0 h devices. Before positive aging, QLEDs might undergo


https://doi.org/10.1021/acsami.4c10646
ACS Appl. Mater. Interfaces XXXX, XXX, XXX−XXX

Table 1. Data for $J$, $L$, and EQE at 4 V with Aging Time for Three Types of Device Structures[a]

| | QD/ZMO/Al | | | QD/PFI/ZMO/Al | | | QD/ZMO/PFI/Al | | |
|---|---|---|---|---|---|---|---|---|---|
| aging time (h) | $J$ (mA/cm$^2$) | $L$ (cd/m$^2$) | EQE (%) | $J$ (mA/cm$^2$) | $L$ (cd/m$^2$) | EQE (%) | $J$ (mA/cm$^2$) | $L$ (cd/m$^2$) | EQE (%) |
| 0 | 463 | 7113 | 3.16 ± 0.28 | 205 | 3181 | 1.81 ± 0.23 | 281 | 4633 | 3.63 ± 0.83 |
| 12 | 685 | 17,524 | 5.45 ± 0.30 | 284 | 22,817 | 5.45 ± 0.66 | 1081 | 32,840 | 7.00 ± 0.39 |
| 24 | 726 | 27,035 | 7.19 ± 0.44 | 624 | 23,325 | 6.04 ± 0.39 | 1090 | 29,642 | 8.89 ± 0.88 |
| 48 | 780 | 29,182 | 7.71 ± 0.62 | 604 | 22,752 | 6.85 ± 0.59 | 848 | 20,913 | 7.01 ± 0.36 |
| 72 | 826 | 32,199 | 9.64 ± 0.42 | 591 | 25,539 | 8.29 ± 0.78 | 1005 | 19,996 | 8.16 ± 0.49 |
| 96 | 892 | 33,383 | 10.8 ± 0.50 | 483 | 23,900 | 11.1 ± 0.88 | 1215 | 24,761 | 10.3 ± 0.94 |
| 120 | 867 | 35,830 | 12.0 ± 0.33 | 466 | 23,376 | 8.84 ± 0.25 | 1216 | 25,227 | 11.3 ± 0.95 |

[a]Average, standard deviation (EQE), and maximum values ($J$, $L$) of the primary characteristics of QLEDs were measured on at least six devices for each device type.

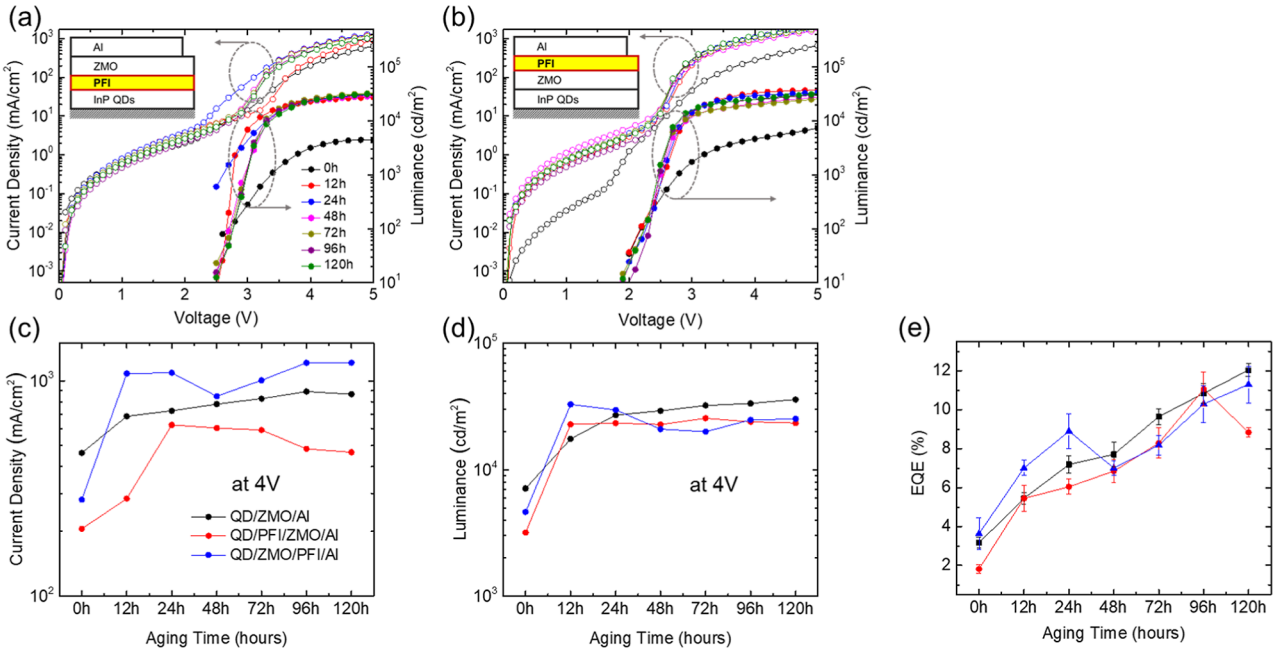


**Figure 2.** $J$–$V$–$L$ characteristics of the device structures of (a) ITO/PEDOT:PSS/TFB/QD/PFI/ZMO/Al and (b) ITO/PEDOT:PSS/TFB/QD/ZMO/PFI/Al. Variations in (c) current density and (d) luminance at 4 V with respect to positive aging time. (e) Maximum EQE trends for each device structure over positive aging time.

nonuniform emission on the luminous area, indicating presence of nonuniform charge transport paths in the device as shown in Figure S1.[23,24] In these devices, charge transport areas are limited, exhibiting low current flow upon the voltage bias (especially on the low voltage regime). The positive aging modifies the charge transport conditions in the devices. The enhanced charge transport eventually results in uniform emission in the luminous pixel area. Therefore, charge transport path in the device enlarged, resulting increase of current density levels (Figure 1c). The gradual increase in EQE from 3.16 to 12.04% over 120 h of aging indicates a substantial enhancement in the efficiency of the QLED device by positive aging (Table 1). Because of the gradual increase in the efficiency, the favorable agent in the resin is speculated to penetrate the device, reacting and enhancing the optoelectrical characteristics of each device constituent layer. The resin was located at the top of the Al electrode, and the positive agents were required to penetrate the Al electrode in the direction of the QD layer. Therefore, a time-dependent analysis of the positive aging of each device constituent layer is imperative to investigate this mechanism. We strategically introduced a PFI interlayer into the device structure to inhibit the interaction at the positioned spots or retard the positive agent penetration into the bottom layers. PFI is one of the materials that act as an insulator and is widely used as a material that is inserted into the interface of HTL to bend the conduction band and the balance band to a deep work function.[25,26] Also, PFI was able to form a thin film while maintaining the integrity of the lower layers in a process. However, the change in device characteristics with respect to the change in work function is limited only to causing the difference in initial light emission characteristics of each device according to the PFI position. In the fundamental role of delaying the resin penetration over time, all devices to which PFI has been applied have the same characteristics. In addition, the thickness of PFI is an important parameter in the electrical performance of the device. As shown in the Figure S2, the maximum EQE of the device of ZMO/PFI/Al structure having a greatly decreases as the PFI thickness increases. This indicates that thick PFI interferes with the electronic transport of the device, reducing the performance of the device. To prevent this, PFI was employed with a very thin thickness (0.05 wt %, 1−2 nm) that does not interfere with the transport of electrons. The operational lifetime was measured to further integrated the properties of


https://doi.org/10.1021/acsami.4c10646
ACS Appl. Mater. Interfaces XXXX, XXX, XXX−XXX

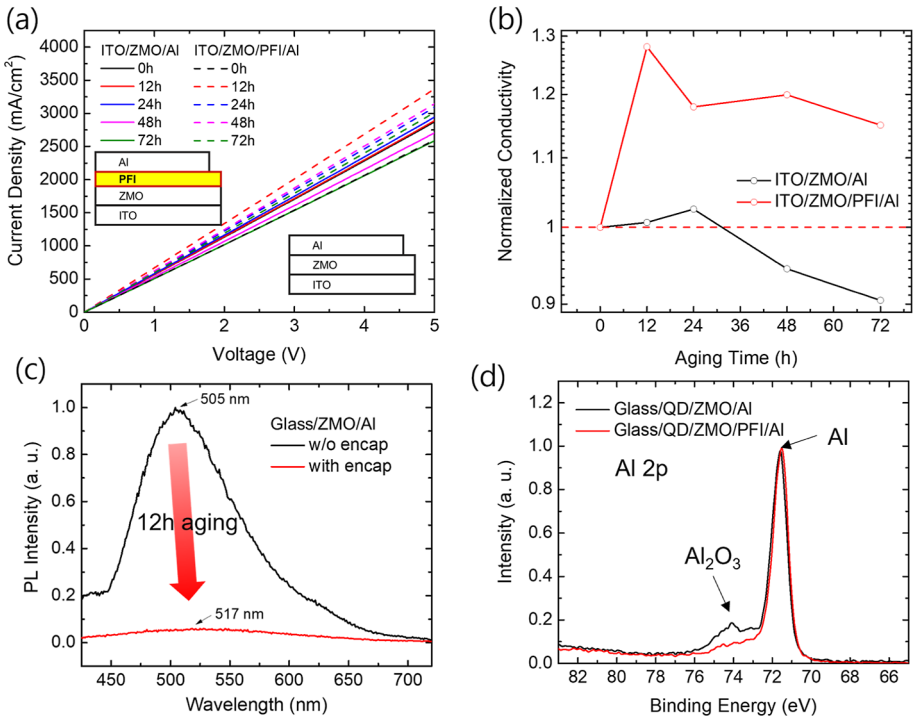


**Figure 3.** (a) Comparative analysis of EOD with and without the PFI over positive aging time: *J*−*V* curve of ITO/ZMO/Al and ITO/ZMO/PFI/Al structures. The dashed lines represent the PFI-inserted devices over aging time. (b) Normalized conductivity of EODs. (c) Changes in steady-state PL of ZMO films after 12 h of aging. (d) Depth profiling of XPS (Al 2p) at the interface of ZMO/Al and ZMO/PFI/Al after 48 h of aging.

PFI interlayers in the devices. As shown in Figure S3, lifetime of ZMO/PFI/Al structure increased after 72 h due to an increase in electron transport properties due to alignment of the ETL work function by PFI along with the conductivity of ZMO improved by the positive aging effect. Lifetime of QD/PFI/ZMO structure decreased by interfering with charge injection as PFI downshifted the energy level and mismatched the work function of QD/ZMO. Thus, the operational lifetime difference according to the PFI position is originated from the changes in the interfacial electrical characteristics other than the original purpose of delaying positive aging.

Based on previous reports, the origin of the positive aging could be attributed to (i) ZMO (ZMO surface passivation) and (ii) ZMO/Al interface ($AlO_x$ formation).[1,9,17,21,22] Furthermore, the positive agents were speculated to affect the QD or QD/ZMO interface. Therefore, the PFI interlayer (1−2 nm) was inserted into the QD/ZMO and ZMO/Al interfaces to investigate the origin of the positive aging mechanism separately. Figure 2a shows how the current density and luminance characteristics of the QLEDs with PFI inserted between the QD and ZMO layers change across aging time. Initially (0 h), the QLEDs demonstrate a sharp increase in current density and luminance at approximately 2.5 V. After 12 h of aging, the current density shows a better diode curve and increases from 205 to 284 mA/cm$^2$ at 4 V, which is an increase of approximately 38.5%. During this time, the luminance at 4 V increases significantly from 3181 to 22,817 cd/m$^2$, marking a significant 617% increase. Figure 2b presents the current density and luminance characteristics in QLEDs with PFI inserted between ZMO and Al layers with aging time. In the initial phase from 0 and 12 h, the current density at 4 V increases from 281 to 1081 mA/cm$^2$, a substantial 285% increase, and the luminance increases from 4633 to 32,840 cd/m$^2$, a remarkable 609% increase, indicating enhanced diode characteristics and light emission efficiency. Despite a reduction in both parameters after 24 h, a positive aging trend becomes apparent over 48 h, culminating with a current density of 1216 mA/cm$^2$, a luminance of 25,227 cd/m$^2$, and an EQE of 11.29% at 120 h. These outcomes suggest that with prolonged aging, the ZMO and QD layers undergo gradual passivation, thereby improving the charge injection balance and radiative recombination efficiency and increasing the luminescence efficiency. Figure 2c exhibits the variation in current density over aging time for each device structure. The QD/ZMO/Al structure (black line) exhibited a consistent increase in current density from an initial 463 to 867 mA/cm$^2$ in 120 h of aging. This result indicates a continual improvement in charge injection and transport efficiency within the device. Conversely, the QD/PFI/ZMO/Al structure (red line) showed an increasing trend to 284 and 624 mA/cm$^2$ after 12 and 24 h of aging, respectively, followed by a decrease to 604 mA/cm$^2$ after 48 h and a gradual reduction to 466 mA/cm$^2$ after 120 h. These observations suggest that while the insertion of the PFI layer initially has a positive effect on charge injection and transport, it may lead to nonradiative recombination or other loss mechanisms over the long-term. For the QD/ZMO/PFI/Al structure (blue line), the current density initially increased from 281 mA/cm$^2$, followed by a remarkable decrease to 848 mA/cm$^2$ after 48 h of aging. However, it subsequently increased again, reaching 1216 mA/cm$^2$ after 120 h, indicating that the position of the PFI layer significantly influences the trend of current density changes with aging time. Figure 2d presents the luminance changes over the aging time for each device structure. The QD/ZMO/Al structure exhibited a continuous increase in luminance, rising from an initial value of 7113 to 35,830 cd/m$^2$ after 120 h of aging. This suggests that the luminance optimization in QLED devices occurs after prolonged aging of over 120 h. In


https://doi.org/10.1021/acsami.4c10646
ACS Appl. Mater. Interfaces XXXX, XXX, XXX−XXX

the QD/PFI/ZMO/Al structure, the luminance increased from an initial 3181 to 25,539 cd/m$^2$ after 72 h of aging and demonstrated stable luminance levels at 23,900 and 23,376 cd/m$^2$ after 96 and 120 h of aging, respectively. The QD/ZMO/PFI/Al structure showed a significant increase to 32,840 cd/m$^2$ after 12 h of aging, followed by a decrease to 20,913 cd/m$^2$ after 48 h and a subsequent increase to 25,227 cd/m$^2$ after 120 h, indicating variability in luminance.

Figure 2e shows the variations in the EQE with aging time for each device structure. The QD/ZMO/Al structure exhibited a consistent improvement in EQE, starting at 3.16% and increasing to 12.04% after 120 h of aging. This indicates a gradual enhancement in the EQE of the device over time. For the QD/PFI/ZMO/Al structure, the EQE began at 1.81% and increased to 11.05% after 96 h of aging but subsequently decreased slightly to 8.84% after 120 h. These results suggest that inserting PFI between the QD and the ZMO initially improves the efficiency but may lead to a decrease over the long-term. For the QD/ZMO/PFI/Al structure, the EQE was initially 3.63% and increased to 11.29% after 120 h. The remarkable decrease in EQE was observed at approximately 48 h, which should be comprehensively investigated. The detailed EQE characteristics, EL spectra and statistical data related to the EQE, current density and luminance of each device structure are shown in Figures S4−S6, respectively (Supporting Information).

The current−voltage ($J$−$V$) characteristics of ZMO-based electron-only devices (EOD) were analyzed with and without the inclusion of PFI to investigate the impact of PFI on the electrical properties of the ZMO/Al interface due to positive aging. Figures 3a and S7 compares the $J$−$V$ measurements of the ITO/ZMO/Al and ITO/ZMO/PFI/Al structures during aging. It was found that the presence of PFI significantly increased the current density over time, whereas the current density was reduced in the case of the ITO/ZMO/Al structure. Introducing PFI can be considered to inhibit $Al_2O_3$ formation at the ZMO/Al interface, because $Al_2O_3$ is an electrical insulator that reduces device conductivity. Figure 3b shows the variations in the conductivity of the devices, demonstrating that adding PFI increased conductivity with aging time. The conductivity ($\sigma$) was calculated based on the thickness of the ZMO thin film ($d$) as well as the voltage ($V$) and current density ($J$) obtained from the EOD measurements using the following relationships: $V = Ed$ and $J = \sigma E$. The introduction of the PFI layer inhibited $Al_2O_3$ formation at the ZMO and Al interface, resulting in enhanced electron conductivity. The conductivity of the ITO/ZMO/Al device showed a slight increase during the initial 24 h, which should have decreased because of $Al_2O_3$ formation. To address this controversy, we can consider defect passivation of ZMO by positive aging.[9,20,21] Oxygen vacancies in ZMO reported to act as donors of ZMO.[27,28] However, the trap states formed by the defects in ZMO are one of the primary causes negatively affecting the luminous efficiency by inducing electron−hole recombination such as nonradiative recombination.[29,30] Figure 3c shows that the impact of these trap states can be significantly reduced through a 12-h aging process. The broad emission at approximately 500 nm exhibits trap emission from the defect states of ZMO. After 12 h of aging, a peak shift from 505 to 517 nm and a notable decrease in the photoluminescence (PL) intensity were observed, indicating effective passivation of the defect states (oxygen vacancy, Oii) on the ZMO surfaces.[19] Because the defect states originated from the oxygen vacancies on the ZMO surface and the oxygen vacancies retarded electron injection with electrical resistivity, the conductivity of the ZMO film increased with the passivation of the defect states in ZMO.[9,19,21] As shown in Figure 3b, during the initial 24 h of aging, the conductivity (in the case of ITO/ZMO/Al) increased with the ZMO defect passivation by positive aging. After 24 h of device aging, the conductivity started to decrease because the effect of ZMO passivation was complete, and the $Al_2O_3$ formation dominantly affected the entire charge transport. Figure 3d presents the depth profile of X-ray photoelectron spectroscopy (XPS). The black line represents the XPS results for glass/QD/ZMO/Al, whereas the red line represents the results for glass/QD/ZMO/PFI/Al after 48 h of aging. In the XPS analysis, the binding energy peaks of $Al_2O_3$ and Al have specific values. In the spectral results, the Al peak was strongly signaled at approximately 72 eV, and the peak of $Al_2O_3$ was more distinctly observed at approximately 74.5 eV.[31−33] The comparison of the two spectra showed that the peak of $Al_2O_3$ near the Al 2p peak is significantly lower in the structure with inserted PFI. This result indicated that PFI insertion inhibited $Al_2O_3$ formation at the ZMO/Al interface. Because the electrons from the Al electrode could be trapped by the defect states in ZMO, the presence of thin and insulating $Al_2O_3$ effectively inhibited the pathway of the injected electrons trapped in the ZMO defect sites. Therefore, $Al_2O_3$ facilitates enhanced charge injection into the QD layer with significantly reduced nonradiative recombination, thus augmenting the overall efficacy of the device. The sequential effects of positive aging could be summarized promptly. In the initial aging stage (~24 h), the ZMO defect states were effectively passivated, resulting in enhanced electron injection into the QD layer. Moreover, defect passivation of ZMO prevents exciton quenching at the QD/ZMO interface, promising enhanced EL from QD.

The results shown in Figure 2c−e could be comprehensively investigated. Because the ZMO defect states were effectively passivated within 24 h of aging, the current density of the devices increased for up to 24 h of aging (Figure 2c). Moreover, as shown in Figure 2d, the luminance of the devices rapidly increased during the initial 12 h owing to the reduced exciton quenching at the QD/ZMO interface. Consequently, during the initial 24 h of aging, the EQEs of the devices increased (Figure 2e). Interestingly, at an aging time of 24−72 h, a remarkable decrease in luminance was observed for the QD/ZMO/PFI/Al device (Figure 2d). As shown in Figure 3d, the insertion of PFI between ZMO and Al inhibits $Al_2O_3$ formation. Thus, the injected electrons from the Al electrode could be captured by the trap states in ZMO, although most of the defect states of ZMO were passivated during the initial stage of aging. These trapped electrons diminish the radiative recombination from the QDs, resulting in reduced luminance. Consequently, the EQE of the QD/ZMO/PFI/Al device decreased after 48−72 h of aging (Figure 2e).

Regardless of $Al_2O_3$ formation, the EQEs of the devices increased after 72 h of aging (Figure 2e). Thus, further positive mechanisms exist for long-term aging (>72 h). According to Keating et al. (2022), although no mixing between the ZnO nanoparticles and QDs has been reported,[34] the possibility of very small ZnO particles infiltrating the QD layer cannot be excluded. These Zn/O species diffusing into the QD layer could contribute to the charging processes that induce overpotentials. As observed by scanning transmission electron microscopy-EDX, the Zn and O species in the QD film were


https://doi.org/10.1021/acsami.4c10646
ACS Appl. Mater. Interfaces XXXX, XXX, XXX−XXX

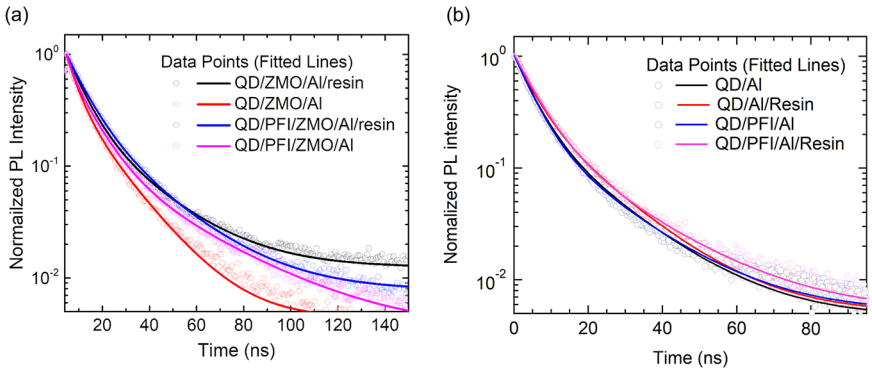


**Figure 4.** Time-resolved PL comparison and results for InP QD-based devices with and without resin. The devices (a) with and (b) without ZMO films were investigated. The data points represent the experimental results, and the solid lines indicate the double-exponential fitting lines. All devices were treated for 48 h of positive aging.

likely derived from the ZnO spin-coating solution, and these charged species might contribute to the slow equilibration in the transient EL and variability among devices. Therefore, the penetration of ZnO and exciton quenching at the QD/ZnO interface could significantly affect the efficiency and lifetime of QLED devices. Our study also confirms that a precise understanding and control of the exciton quenching phenomena at the ZMO and QD layer interfaces are critical for developing high-efficiency QLED devices.[34,35]

Figure 4 shows the time-resolved PL (TRPL) results. The films were formed based on the presence of resin (positive aging) and the use of PFI, and the measurements were performed after 48 h of aging. Data points were fitted using a double-exponential function, $y = \alpha_1 \exp\left(\frac{-t_1}{\tau_1}\right) + \alpha_2 \exp\left(\frac{-t_2}{\tau_2}\right)$, through which the average PL lifetime, $\tau_{avg} = \frac{\alpha_1\tau_1^2 + \alpha_2\tau_2^2}{\alpha_1\tau_1 + \alpha_2\tau_2}$, is defined based on the fitting of the PL data points. Table 2 presents the quantitative values related to PL decay, including the pre-exponential factors ($\alpha_1$, $\alpha_2$), decay constants ($\tau_1$, $\tau_2$), and calculated average PL lifetime ($\tau_{avg}$). The PL lifetime of the QD/ZMO/Al device structure was calculated to be approximately 12.32 ns, which increased significantly to 16.86 ns owing to the positive aging effect (QD/ZMO/Al/resin). The significant enhancement (37%) of the PL lifetime originates from the combined effect of the passivation of ZMO and QD. As shown in Figure 3c, the PL quenching sites were passivated by positive aging, which enhanced the PL lifetime of the QD/ZMO/Al/resin device. Moreover, the exciton dynamics at the large interfacial area between QD/ZMO are significantly affected by the reduced exciton quenching sites on the ZMO surfaces. Additionally, the exciton quenching sites on the QD surfaces (such as QD-ligand-linked spots) are further passivated by positive aging. A PFI interlayer was inserted between QD and ZMO to separate the impact of ZMO passivation from that of positive aging. Because the insulating PFI was located at the QD−ZMO interface, exciton quenching by the trap states of ZMO was minimized. The QD/PFI/ZMO/Al device structure exhibited a PL lifetime of 14.03 ns. Compared to the QD/ZMO/Al device structure, the PL lifetime increased by approximately 14%. Preventing the ZMO penetration into the QD layer (by inserting PFI) effectively reduced the interfacial area between QD/ZMO. The QD and ZMO layers were completely separated. Because the devices were not encapsulated with resin, the enhancement of the PL lifetime could be interpreted as an effect of the separation of exciton quenching sites on ZMO from the QD surfaces. Furthermore, the positive aging of the QD/PFI/ZMO/Al/resin device structure showed a PL lifetime of 16.06 ns.

**Table 2. TRPL Fitting Results for InP QD-Based Films with and without Resin**

| | $\alpha_1$ | $\alpha_2$ | $\tau_1$ (ns) | $\tau_2$ (ns) | $\tau_{avg}$ (ns) |
|---|---|---|---|---|---|
| QD/ZMO/Al/resin | 0.68 | 0.32 | 7.15 | 23.21 | 16.86 |
| QD/ZMO/Al | 0.62 | 0.38 | 4.76 | 15.99 | 12.32 |
| QD/PFI/ZMO/Al/resin | 0.73 | 0.27 | 8.13 | 23.49 | 16.06 |
| QD/PFI/ZMO/Al | 0.61 | 0.39 | 4.97 | 17.95 | 14.03 |
| QD/Al/resin | 0.68 | 0.32 | 4.97 | 15.52 | 11.27 |
| QD/Al | 0.76 | 0.24 | 4.83 | 16.40 | 10.84 |
| QD/PFI/Al/resin | 0.80 | 0.20 | 5.78 | 19.32 | 11.99 |
| QD/PFI/Al | 0.79 | 0.21 | 4.86 | 17.36 | 10.90 |

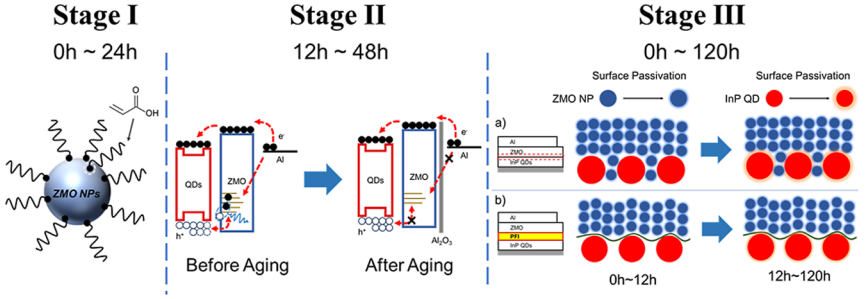


**Figure 5.** Time-resolved positive aging mechanism of QLEDs: (I) 0−24 h, defect passivation on the ZMO surfaces; (II) 12−48 h, $Al_2O_3$ formation at the ZMO/Al interface; (III) 0−120 h, defect passivation on the exciton quenching site on the QD surfaces.


https://doi.org/10.1021/acsami.4c10646
ACS Appl. Mater. Interfaces XXXX, XXX, XXX−XXX

Compared with the QD/PFI/ZMO/Al device structure, the PL lifetime increased by approximately 14%. Thus, the increase in the PL lifetime originates from the reduced exciton quenching sites on the QD owing to the positive aging effect. In particular, the strong $\alpha_1$ parameter (0.73) indicates that most excitons in the QD layer show direct recombination rather than delayed emissions. To further investigate the positive aging effect on the QD, the TRPL of single QD/Al films with and without resin was investigated (Figure 4b). The QD/Al/resin device structure exhibited a PL lifetime of 11.27 ns. Compared to the QD/Al device structure, the PL lifetime increased by approximately 4%. Moreover, the PL lifetime of the QD/PFI/Al/resin device structure showed a further increase to 11.99 ns, which is a 10% enhancement from the QD/PFI/Al device structure. Thus, the increase in the PL lifetime originated from the reduced number of exciton quenching sites on the QD surface owing to the positive aging effect. Therefore, with respect to aging time, the positive agents from the encapsulation resin effectively passivated the exciton quenching sites on QD, ZMO, and their interfaces.

Figure 5 illustrates a diagram that explains the temporal microscopic changes occurring at the film interfaces and their interactions during positive aging. In **Stage I** (0−24 h), the primary focus was on the passivation effect of the ZMO layer by positive aging, which was common across all device structures. Resin-mediated surface passivation of ZMO significantly reduces the electrical resistivity and nonradiative recombination at the QD/ZMO interface, leading to enhanced current density, luminance, and EQE of the devices. This improvement marks an initial boost in QLED performance and underscores the importance of nanoscale surface passivation in influencing the luminescence characteristics of QLED devices, thereby boosting their efficiency and stability.

**Stage II** (12−48 h) highlights shifts in the electron and hole injection characteristics at the ZMO/Al interface. The QD/ZMO/PFI/Al structure demonstrates that the PFI layer insertion suppressed $Al_2O_3$ formation, translating into an early electrical conductivity improvement (Figure 3b). The penetration of positive agents at the ZMO/Al interface tends to accelerate $Al_2O_3$ formation, with the created $Al_2O_3$ layer preventing nonradiative recombination at the trap states in ZMO, thereby impacting the aging performance of the QLEDs. The combined effect of ZMO passivation and $Al_2O_3$ formation significantly inhibits exciton quenching from ZMO. **Stage III** (0−120 h) marks the final stage of the positive aging mechanism, characterized by the resin-accelerated passivation processes of ZMO and QD. The PFI at the QD/ZMO interface mitigates the adverse interactions between the QD and ZMO layers. Furthermore, the exciton quenching states (on the QD or QD/ZMO interfaces) could be effectively passivated by the positive agents from the resin over the aging time. Therefore, the devices exhibit a steady enhancement in EL performance over time. In summary, the timely but combined effect of defect passivation of ZMO, QD, and their interfaces with $Al_2O_3$ formation significantly enhances the EL performance of InP QLEDs. These stages collectively demonstrate the significant roles played by the film interface composition, passivation mechanisms, and effects of interfacial interactions.

## CONCLUSION

The positive aging mechanism of QLED devices facilitated by UV-curable resins was systematically investigated. To determine the effect of the UV-curable resin on ETL and EML, the long-term characteristics were analyzed over 120 h by inserting a PFI insulating interlayer between the electrode and ETL (QD/ZMO/PFI/Al) and between ETL and EML (QD/PFI/ZMO/Al). The PFI insertion delayed the $Al_2O_3$ formation at the ZMO/Al interface and reduced the contact between the QD and ZMO at the QD/ZMO interface, thereby inhibiting exciton quenching at the spots. The encapsulation with the UV-curable resin successfully passivated the ZMO surfaces, as indicated by the decrease in the PL spectrum of ZMO after 12 h of aging. Additionally, the UV-curable resin facilitated the reaction of Al with oxygen from ZMO, forming $Al_2O_3$, as evidenced by XPS. Moreover, the UV-curable resin passivated the QD surface to inhibit the nonradiative recombination at the QD/ZMO interface, reducing PL quenching. Owing to the enhanced electron injection and suppression of exciton quenching, the 120-h aged InP QLEDs exhibited enhanced EQEs of 12.04%, which improved from 3.16% of the control device. This study provides an advanced time-resolved mechanism of positive aging by resin, which is expected to offer valuable insights into exciton dynamics in QLED physics.

## EXPERIMENTAL SECTION

**Materials.** PEDOT:PSS (AI4083) was purchased from Heraeus. Zinc acetate [$Zn(Ac)_2$ > 99.9%] and magnesium acetate tetrahydrate [$Mg(Ac)_2$ $4H_2O$, 99%] were purchased from Alfa Aesar. Tetramethylammonium hydroxide pentahydrate (TMAH > 97%), poly[(9,9-dioctylfluorenyl-2,7-diyl)-*co*-(4,4-(*N*-(4-*sec*-butylphenyl)-diphenylamine))] (TFB), ethanol, acetone, hexane, dimethyl sulfoxide, isopropyl alcohol (IPA), and chlorobenzene were purchased from Sigma-Aldrich. All chemicals were used as received.

The synthesis of the core, InP/ZnSe/ZnS QDs, and ZMO, followed a previously reported process without modification.[36]

**Device Fabrication.** The ITO-patterned glass was cleaned separately with acetone, IPA, and deionized water. The ITO substrates were subsequently treated with UV/ozone for 30 min. PEDOT:PSS was filtered (HP, 0.45 $\mu$m) and spin coated (3000 rpm, 60 s) onto substrates, followed by annealing at 130 °C for 20 min in air. The substrates were transferred to an $N_2$-filled glovebox for further fabrication. A 7 mg/mL solution of TFB dissolved in chlorobenzene was spin coated on the PEDOT:PSS layer at 4000 rpm for 30 s and annealed at 150 °C for 30 min. After cooling to room temperature, the QD (InP−ZnSe−ZnS) in octane was spin coated at 3000 rpm for 30 s and annealed at 70 °C for 30 min. For the PFI-inserted devices, the 0.05 wt % PFI in IPA was spin coated at 5000 rpm for 30 s and annealed at 70 °C for 30 min. The ZMO solution was spin coated at 4000 rpm for 30 s and annealed at 70 °C for 30 min. Finally, 100 nm of Al was thermally evaporated at a rate of 1−2 A $s^{-1}$ under 3.0 × $10^{-6}$ Torr. The devices were encapsulated in a cover glass after fabrication.

**Positive Aging Method.** The QLED was encapsulated by UV-curable resin (Loctite, AA 366). After being dropped on top of the devices, the UV-curable resin was covered with a cover glass. The devices were cured using UV lamps (365 and 405 nm) for 1 min. The positive aging process was conducted by annealing the resin-encapsulated devices at 70 °C. Aging was conducted in a $N_2$-filled glovebox, and the EL measurements were conducted at 12-h intervals up to the first 24 h and at 24-h intervals thereafter.

**Device Characterization.** The electrical performance and emission properties of the devices were analyzed by measuring their current−voltage−luminance characteristics by using a CS-2000 spectroradiometer (Minolta) and their EL spectra by using a Keithley 2450 source meter. XPS analysis was conducted using a photoelectron spectrometer (NEXSA, Thermo Fisher Scientific) to study the surface chemistry and elemental composition of the QLED components. The


https://doi.org/10.1021/acsami.4c10646
ACS Appl. Mater. Interfaces XXXX, XXX, XXX−XXX

steady-state PL and TRPL measurements were performed using a fluorescence spectrometer (FluoTime 300, PicoQuant).

## ■ ASSOCIATED CONTENT

### Supporting Information

The Supporting Information is available free of charge at https://pubs.acs.org/doi/10.1021/acsami.4c10646.

Emission area of before and after positive aging. Maximum EQE of the device for different PFI concentration. Luminance versus time of QLEDs. EQE trends and EL spectrum over aging time for the device structures. Statistical data related to the EQE, current density, and luminance of the devices. $J-V$ curve of EOD with and without the PFI (PDF).

## ■ AUTHOR INFORMATION


### Corresponding Authors

**Sang-Shin Lee** − *Nano Device Application Center, Department of Electronic Engineering, Kwangwoon University, Seoul 01897, Republic of Korea;* orcid.org/0000-0001-5686-4893; Email: slee@kw.ac.kr

**Hyunho Lee** − *Nano Device Application Center, Department of Electronic Engineering, Kwangwoon University, Seoul 01897, Republic of Korea;* orcid.org/0000-0002-7602-1639; Email: hyunho@kw.ac.kr

### Authors

**Sung-Yoon Joe** − *Nano Device Application Center, Department of Electronic Engineering, Kwangwoon University, Seoul 01897, Republic of Korea*

**Beomhee Yoon** − *Nano Device Application Center, Department of Electronic Engineering, Kwangwoon University, Seoul 01897, Republic of Korea*

**Doyoon Shin** − *SKKU Advanced Institute of Nanotechnology (SAINT), Sungkyunkwan University, Suwon 16419, Republic of Korea*

**Wan Ki Bae** − *SKKU Advanced Institute of Nanotechnology (SAINT), Sungkyunkwan University, Suwon 16419, Republic of Korea;* orcid.org/0000-0002-3832-2449

Complete contact information is available at: https://pubs.acs.org/10.1021/acsami.4c10646


### Author Contributions

[§]S.-Y.J. and B.Y. contributed equally. The manuscript was written through the contributions of all authors. All the authors approved the final version of the manuscript.

### Notes

The authors declare no competing financial interest.

## ■ ACKNOWLEDGMENTS

This research was supported by the Core Research Institute Basic Science Research Program through the National Research Foundation of Korea (NRF), funded by the Ministry of Education (no. 2018R1A6A1A03025242). This work was supported by the Basic Science Research Program (NRF-2022R1F1A1066526) through the National Research Foundation of the Ministry of Education, Republic of Korea.

## ■ ABBREVIATIONS

EML, emission material layer; EOD, electron-only device; EQE, external quantum efficiency; ETL, electron transport layer; PFI, perfluorinated ionomer; PL, photoluminescence; QD, quantum dot; QLED, quantum-dot light-emitting diode; TRPL, time-resolved PL; XPS, X-ray photoelectron spectroscopy; ZMO, zinc magnesium oxide

## ■ REFERENCES


(1) Mashford, B. S.; Stevenson, M.; Popovic, Z.; Hamilton, C.; Zhou, Z.; Breen, C.; Steckel, J.; Bulovic, V.; Bawendi, M.; Coe-Sullivan, S.; et al. High-Efficiency Quantum-Dot Light-Emitting Devices with Enhanced Charge Injection. *Nat. Photonics* **2013**, *7* (5), 407−412.

(2) Zhang, H.; Chen, S.; Sun, X. W. Efficient Red/Green/Blue Tandem Quantum-Dot Light-Emitting Diodes with External Quantum Efficiency Exceeding 21%. *ACS Nano* **2018**, *12* (1), 697−704.

(3) Yang, Y.; Zheng, Y.; Cao, W.; Titov, A.; Hyvonen, J.; Manders, J. R.; Xue, J.; Holloway, P. H.; Qian, L. High-efficiency Light-Emitting Devices Based on Quantum Dots with Tailored Nanostructures. *Nat. Photonics* **2015**, *9* (4), 259−266.

(4) Kim, H.-M.; Kim, J.; Jang, J. Quantum-Dot Light-Emitting Diodes with a Perfluorinated Ionomer-Doped Copper-Nickel Oxide Hole Transporting Layer. *Nanoscale* **2018**, *10* (15), 7281−7290.

(5) Peng, H.; Jiang, Y.; Chen, S. Efficient Vacuum-Free-Processed Quantum Dot Light-Emitting Diodes with Printable Liquid Metal Cathodes. *Nanoscale* **2016**, *8* (41), 17765−17773.

(6) Cao, W.; Xiang, C.; Yang, Y.; Chen, Q.; Chen, L.; Yan, X.; Qian, L. Highly Stable QLEDs with Improved Hole Injection via Quantum Dot Structure Tailoring. *Nat. Commun.* **2018**, *9* (1), 2608.

(7) Dai, X.; Zhang, Z.; Jin, Y.; Niu, Y.; Cao, H.; Liang, X.; Chen, L.; Wang, J.; Peng, X. Solution-Processed, High-Performance Light-Emitting Diodes Based on Quantum Dots. *Nature* **2014**, *515* (7525), 96−99.

(8) Cao, F.; Wang, H.; Shen, P.; Li, X.; Zheng, Y.; Shang, Y.; Zhang, J.; Ning, Z.; Yang, X. High-Efficiency and Stable Quantum Dot Light-Emitting Diodes Enabled by a Solution-Processed Metal-Doped Nickel Oxide Hole Injection Interfacial Layer. *Adv. Funct. Mater.* **2017**, *27* (42), 1704278.

(9) Su, Q.; Sun, Y.; Zhang, H.; Chen, S. Origin of Positive Aging in Quantum-Dot Light-Emitting Diodes. *Adv. Sci.* **2018**, *5* (10), 1800549.

(10) Shen, H.; Cao, W.; Shewmon, N. T.; Yang, C.; Li, L. S.; Xue, J. High-Efficiency, Low Turn-on Voltage Blue-Violet Quantum-Dot-Based Light-Emitting Diodes. *Nano Lett.* **2015**, *15* (2), 1211−1216.

(11) Colvin, V. L.; Schlamp, M. C.; Alivisatos, A. P. Light-Emitting Diodes Made from Cadmium Selenide Nanocrystals and a Semiconducting Polymer. *Nature* **1994**, *370* (6488), 354−357.

(12) Shen, H.; Gao, Q.; Zhang, Y.; Lin, Y.; Lin, Q.; Li, Z.; Chen, L.; Zeng, Z.; Li, X.; Jia, Y.; Wang, S.; Du, Z.; Li, L. S.; Zhang, Z. Visible Quantum Dot Light-Emitting Diodes with Simultaneous High Brightness and Efficiency. *Nat. Photonics* **2019**, *13* (3), 192−197.

(13) Kim, T.; Kim, K.-H.; Kim, S.; Choi, S.-M.; Jang, H.; Seo, H.-K.; Lee, H.; Chung, D.-Y.; Jang, E. Efficient and Stable Blue Quantum Dot Light-Emitting Diode. *Nature* **2020**, *586* (7829), 385−389.

(14) Li, X.; Lin, Q.; Song, J.; Shen, H.; Zhang, H.; Li, L. S.; Li, X.; Du, Z. Quantum-Dot Light-Emitting Diodes for Outdoor Displays with High Stability at High Brightness. *Adv. Opt. Mater.* **2020**, *8* (2), 1901145.

(15) Jang, E.; Kim, Y.; Won, Y.-H.; Jang, H.; Choi, S.-M. Environmentally Friendly InP-Based Quantum Dots for Efficient Wide Color Gamut Displays. *ACS Energy Lett.* **2020**, *5* (4), 1316−1327.

(16) Yoon, S.-Y.; Lee, Y.-J.; Yang, H.; Jo, D.-Y.; Kim, H.-M.; Kim, Y.; Park, S. M.; Park, S.; Yang, H. Performance Enhancement of InP Quantum Dot Light-Emitting Diodes via a Surface-Functionalized ZnMgO Electron Transport Layer. *ACS Energy Lett.* **2022**, *7* (7), 2247−2255.

(17) Chrzanowski, M.; Zatryb, G.; Sitarek, P.; Podhorodecki, A. Effect of Air Exposure of ZnMgO Nanoparticle Electron Transport

Layer on Efficiency of Quantum-Dot Light-Emitting Diodes. *ACS Appl. Mater. Interfaces* **2021**, *13* (17), 20305−20312.
(18) Sun, Y.; Jiang, Y.; Peng, H.; Wei, J.; Zhang, S.; Chen, S. Efficient Quantum Dot Light-Emitting Diodes with a Zn 0.85 Mg 0.15 O Interfacial Modification Layer. *Nanoscale* **2017**, *9* (26), 8962−8969.
(19) Chen, J.; Ghorbani, A.; Chung, D. S.; Azadinia, M.; Davidson-Hall, T.; Chun, P.; Lyu, Q.; Cotella, G.; Song, D.; Xu, Z.; et al. Influence of Encapsulation on the Efficiency and Positive Aging Behavior in Blue Quantum Dot Light-Emitting Devices. *ACS Appl. Mater. Interfaces* **2023**, *15* (28), 34240−34248.
(20) Acharya, K. P.; Titov, A.; Hyvonen, J.; Wang, C.; Tokarz, J.; Holloway, P. H. High Efficiency Quantum Dot Light Emitting Diodes from Positive Aging. *Nanoscale* **2017**, *9* (38), 14451−14457.
(21) Chen, Z.; Su, Q.; Qin, Z.; Chen, S. Effect and Mechanism of Encapsulation on Aging Characteristics of Quantum-Dot Light-Emitting Diodes. *Nano Res.* **2021**, *14*, 320−327.
(22) Li, Z. Enhanced Performance of Quantum Dots Light-Emitting Diodes: The Case of Al2O3 Electron Blocking Layer. *Vacuum* **2017**, *137*, 38−41.
(23) Jin, W.; Deng, Y.; Guo, B.; Lian, Y.; Zhao, B.; Di, D.; Sun, X.; Wang, K.; Chen, S.; Yang, Y.; Cao, W.; Chen, S.; Ji, W.; Yang, X.; Gao, Y.; Wang, S.; Shen, H.; Zhao, J.; Qian, L.; Li, F.; Jin, Y. On the Accurate Characterization of Quantum-Dot Light-Emitting Diodes for Display Applications. *npj Flexible Electron.* **2022**, *6* (1), 35.
(24) Li, N.; Lv, Y.; Wang, L.; Li, J.; He, Y.; Fan, J.; Xing, H.; Shen, H.; Zhang, X.; Li, L. S. Optimizing Device Efficiency and Lifetime through Positive Ageing in Quantum Dot Light-Emitting Diodes. *ACS Photonics* **2023**, *10* (8), 2720−2729.
(25) Gangishetty, M. K.; Hou, S.; Quan, Q.; Congreve, D. N. Reducing Architecture Limitations for Efficient Blue Perovskite Light-Emitting Diodes. *Adv. Mater.* **2018**, *30* (20), 1706226.
(26) Kim, H. G.; Kim, M.; Kim, S. S.; Paek, S. H.; Kim, Y. C. Silver Nanowire/PEDOT: PSS Hybrid Electrode for Flexible Organic Light-Emitting Diodes. *J. Sci.: Adv. Mater. Devices* **2021**, *6* (3), 372−378.
(27) Jin, B. J.; Bae, S. H.; Lee, S. Y.; Im, S. Effects of Native Defects on Optical and Electrical Properties of ZnO Prepared by Pulsed Laser Deposition. *Mater. Sci. Eng., B* **2000**, *71* (1−3), 301−305.
(28) Look, D. C.; Reynolds, D. C.; Sizelove, J. R.; Jones, R. L.; Litton, C. W.; Cantwell, G.; Harsch, W. C. Electrical Properties of Bulk ZnO. *Solid State Commun.* **1998**, *105* (6), 399−401.
(29) Polydorou, E.; Zeniou, A.; Tsikritzis, D.; Soultati, A.; Sakellis, I.; Gardelis, S.; Papadopoulos, T. A.; Briscoe, J.; Palilis, L. C.; Kennou, S.; et al. Surface Passivation Effect by Fluorine Plasma Treatment on ZnO for Efficiency and Lifetime Improvement of Inverted Polymer Solar Cells. *J. Mater. Chem. A* **2016**, *4* (30), 11844−11858.
(30) Van Dijken, A.; Meulenkamp, E.; Vanmaekelbergh, D.; Meijerink, A. Identification of the Transition Responsible for the Visible Emission in ZnO Using Quantum Size Effects. *J. Lumin.* **2000**, *90* (3−4), 123−128.
(31) Yoon, K. H.; Kim, H.; Koo Lee, Y. E.; Shrestha, N. K.; Sung, M. M. UV-Enhanced Atomic Layer Deposition of Al 2 O 3 Thin Films at Low Temperature for Gas-Diffusion Barriers. *RSC Adv.* **2017**, *7* (10), 5601−5609.
(32) Greczynski, G.; Hultman, L. X-ray Photoelectron Spectroscopy: towards Reliable Binding Energy Referencing. *Prog. Mater. Sci.* **2020**, *107*, 100591.
(33) Vitanov, P.; Stefanov, P.; Harizanova, A.; Ivanova, T. XPS Characterization of Thin $(Al_2O_3)_x(TiO_2)_{1-x}$ Films Deposited on Silicon. *J. Phys. Conf. Ser.* **2008**, *113*, 012036.
(34) Keating, L. P.; Lee, H.; Rogers, S. P.; Huang, C.; Shim, M. Charging and Charged Species in Quantum Dot Light-Emitting Diodes. *Nano Lett.* **2022**, *22* (23), 9500−9506.
(35) Kim, J.; Hahm, D.; Bae, W. K.; Lee, H.; Kwak, J. Transient Dynamics of Charges and Excitons in Quantum Dot Light-Emitting Diodes. *Small* **2022**, *18* (29), 2202290.
(36) Heo, D.; Chang, J. H.; Shin, D.; Kwak, J.; Bae, W.; Lee, H. Modified Zinc Magnesium Oxide for Optimal Charge-Injection Balance in InP Quantum Dot Light-Emitting Diodes. *Adv. Opt. Mater.* **2023**, *11* (10), 2202256.


https://doi.org/10.1021/acsami.4c10646
*ACS Appl. Mater. Interfaces* XXXX, XXX, XXX−XXX